FRACTOGRAPHIC AND MECHANICAL PROPERTIES OF ALLOY AA7075 SUBJECTED TO T6, T7 AND RRA HEAT TREATMENTS

María del V. Valera y Ney J. Luiggi A.*

Grupo Física de Metales, Departamento de Física. Núcleo de Sucre. Universidad de Oriente. Cumaná. Venezuela.

**e-mail: mvalera05@gmail.com*

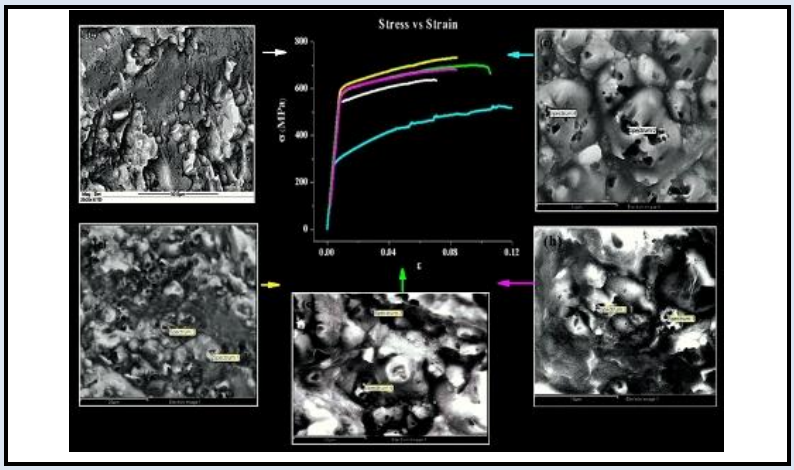

ABSTRACT

This research presents a fractographic study of the AA7075 alloy subjected to T6, T7 and RRA heat treatments and how these thermal procedures affect its mechanical properties. The samples were evaluated by tensile tests; their fractography, through scanning electron microscopy (SEM). All treatments generated an increase in mechanical strength, the T6 effect being largest due to the fine precipitation of η' particles in the matrix, although the ductility and toughness of the AA7075-T6 alloy decreased with respect to their equivalent values in the untreated sample. The highest toughness values reported for the T7 treatment concur with those published by other researchers. Properties during the Retrogression and Re-Aging treatment (RRA) cycles were intermediate to that obtained with the T6 and T7 treatments. The fracture surface fractography revealed differences predicated on the microstructural condition. For all the thermal treatments, the reported failure was of a transgranular character, typical of ductile materials. A wide and irregular distribution of micro dimples and precipitates was evinced depending on the heat treatment applied, the precipitates being distributed over the entire fracture surface. The mechanism responsible for this failure is the formation, growth, and coalescence of micro dimples, although this mechanism seemed to be more complex in the untreated samples due to the abundant presence of defects. Our results seem to indicate that the larger the number of micro dimples, the lower the ductility of the sample and the higher its mechanical strength.

Palabras Claves: *Fractography, Mechanical Properties, AA7075, Heat Treatments.*

Recibido: 24-11-22 ; **Revisado:** 10-06-23

Aceptado: 13-10-23 ; **Publicado:** 10-12-23

https://doi.org/10.5281/zenodo.10557417

pISSN: 0255-6952 | eISSN: 2244-7113

Rev. LatinAm. Metal. Mat. 2023; **43** (1): 19-36

FRACTOGRAFÍAS Y PROPIEDADES MECÁNICAS DE LA ALEACIÓN AA7075 SOMETIDA A LOS TRATAMIENTOS TÉRMICOS T6, T7 Y RRA

RESUMEN

Esta investigación presenta un estudio fractográfico de la aleación AA7075 sometida a los tratamientos térmicos T6, T7 y RRA, y cómo estos procedimientos térmicos afectan sus propiedades mecánicas. Las muestras fueron evaluadas mediante ensayos de tracción; su fractografía mediante Microscopía Electrónica de Barrido (SEM). Todos los tratamientos generaron un incremento en la resistencia mecánica, siendo mayor el efecto T6 debido a la fina precipitación de partículas η' en la matriz, aunque la ductilidad y tenacidad de la aleación AA7075-T6 disminuyó con respecto a sus valores equivalentes en la muestra sin tratar. Los valores de dureza más altos informados para el tratamiento T7 concuerdan con los publicados por otros investigadores. Las propiedades durante los ciclos de tratamiento RRA (Retrogresión y Re–Envejecimiento) fueron intermedias a las obtenidas con los tratamientos T6 y T7. La fractografía de la superficie de fractura reveló diferencias basadas en la condición microestructural. Para todos los tratamientos térmicos, la falla reportada fue de carácter transgranular, típica de materiales dúctiles. Se evidenció una distribución amplia e irregular de microhoyuelos y precipitados dependiendo del tratamiento térmico aplicado, estando los precipitados distribuidos sobre toda la superficie de fractura. El mecanismo responsable de esta falla es la formación, crecimiento y coalescencia de microhoyuelos, aunque este mecanismo parece ser más complejo en las muestras no tratadas debido a la abundante presencia de defectos. Nuestros resultados parecen indicar que cuanto mayor es el número de microhoyuelos, menor es la ductilidad de la muestra y mayor su resistencia mecánica.

Keywords: *Fractografía, Propiedades Mecánicas, AA7075, Tratamientos Térmicos.*

1. INTRODUCCIÓN

The optimization of mechanical properties in the 7000 series is a topic that has captivated many researchers due to the industrial importance of these alloys. The T6, T7, and RRA heat treatments act as microstructure controllers, regulating the type, shape, distribution, and quantity of precipitated phases; and exerting direct incidence on the established mechanical standards.

In recent studies published by the authors [1,2], a DSC kinetic analysis confirmed the phase precipitation sequence and the respective activation energies for each of the heat treatments indicated.

In the work at hand, we will refer to the study of the mechanical properties deduced from tensile tests and how these properties are enhanced by heat treatment. Furthermore, by means of fractographic analyses, we will study how these treatments affect the fracture surfaces and their relationship with the mechanical properties.

The literature is extensive on this subject, although there is still ambiguity about the propagation mechanisms of these microstructural defect. Fractography, despite being an old technique, has now become with the advance of technology, a tool capable of scrutinizing the origin and development of intergranular and transgranular cracks and other elements that negatively affect structures. We refer readers to the works of Bhandarkar and Lisagor [3], Lynch and Moutsos [4], and the very recent short review by Pantazopoulos [5] and the references cited therein.

In this context, regarding the study of AA7075, Hunter and McMillan [6] used tempers T651 and T7351, performing fractographic and microstructural studies on this alloy, to relate the microstructure, fracture topology, and mechanical and fracture properties. They reported that the T7351 temper gave the alloy lower yield strength, smaller and more numerous fracture dimples, and a completely transgranular fracture path, whereas the T651 temper generated higher yield strength, fewer and larger dimples, and a partially intergranular fracture path.

Kirman [7] investigated the effects of heat treatment on the fracture behavior of an aged 7075 aluminum alloy sheet and found that the toughness decreased as the yield stress or yield strength (YS) increased. The decrease in toughness with increasing aging time went in tandem with a change in fracture mode, predominantly from transgranular to intergranular. Microstructural variables such as the width of precipitate-free zones and the nature of the matrix precipitate have no controlling effect on toughness in the aged alloy.

Bhandarkar and Lisagor [3] made a systematic study of fracture behavior in relation to its microstructure under controlled loads on various 7075-T651 aluminum alloys, concluding that grain structure, size, and precipitate distribution, including the type of load testing, considerably affect fracture morphology. A high density of particles of different stoichiometry was detected in bands and in the vicinity of grain joints. These particles were commonly observed as fragmented fracture surfaces of pre-cracked samples with bent notches but were rare on fracture surfaces of plate tension samples.

Irisarri and Atxaga [8] studied the influence of second-phase particles on the fracture behavior of two high strength aluminum alloys (7475 and 7050) under tempers T7351 and T7651, revealing that all fracture surfaces were covered by ductile dimples pointing towards coalescence of micro voids as an operating mechanism, evincing the important role played by second phase particles. Most of these particles were rich in iron, the other elements varying in content.

Zhihui et al. [9] by means of two aging treatments (115 and 160 ºC), investigated the microstructural evolution and the mechanical properties of the AA7075 alloy. The results showed that the first stage of the aging treatment (115°C) dominated the formation of GPI and GPII zone precipitates and favored an increase in the elastic strain of the alloy. After aging for 7 h, the value of the Ultimate Tensile Strength (UTS) was 529 MPa and the precipitates at the grain boundaries were very fine and continuously distributed. During the second aging step at 160°C the maximum strength value was reached for a short time (approximately 12 h) and then the UTS decreased after aging for 36 h, reaching the value 493 MPa. After aging the alloy for 12 h, the UTS value was 530 MPa and the microstructure of the alloy at this stage revealed the presence of η and η' phases and, to a lesser extent, the presence of GPII zones. After aging the alloy at 160 °C for 36 h, they observed many η and η' precipitated phases.

Panigrahi and Jayaganthan [10] studied the mechanical properties of alloy Al7075 rolled at

cryogenic and room temperatures, showing that the suppression of dynamic recovery and the accumulation of a high density of dislocations at cryogenic temperatures enhanced the hardness and mechanical strength of the alloy.

Tajally et al. [11] subjected annealed 7075 alloy samples to cold rolling and showed that this treatment significantly increased the yield strength (YS) due to the resulting higher dislocation density, increasing ultimate tensile strength (UTS) and hardness, but decreasing ductility. The variation in ductility was found to correlate with the fractographic results of specimens subjected to tension and bending. Fractography of the deformed specimens showed a fracture surface with regions of quasi-cleavage and absence of dimples, reflecting a brittle fracture mechanism.

Pedersen et al. [12] investigated the fracture behavior of the AA7075-T651 aluminum alloy for quasi-static and dynamic loading conditions and for different stress states using optical and scanning electron microscopy techniques. The fracture surface obtained in tests with smooth axisymmetric specimens indicates that crack growth is partly intergranular along grain boundaries or precipitation-free zones, and partly interspersed with voids around fine particles and coarse intermetallics.

Askari-Paykani et al. [13] studied the effects of T6 and T73 heat treatments on the microstructural changes and corrosion behavior in the Al7045 alloy and thus confirmed the already established results regarding the presence and majority distribution of η' (T6) and η (T7) phases within the grain and the minority distribution at the contours, as well as the presence of Fe/Cu/Si - and Mg/S -rich intermetallics for T6, and Fe/Cu for T7 at the grain junctions.

Carvalho et al. [14] studied the effects of retro-aging and heat treatment interruption (T7451 and T6I4-65) of the AA7050 aluminum alloy on its fatigue behavior and fatigue crack growth rate, thus demonstrating the effect of second phase particles on these properties and underlining the importance of thermo-mechanical treatments in the control of the microstructure and mechanical properties of aluminum alloys. In addition, by means of SEM fractography, they visualized the striations associated with the advancement of the crack front in individual cycles, correlating them with the overall crack growth rate and crack propagation conditions.

Li et al. [15] optimized the Retrogression and Re-Aging treatment (RRA) parameters to improve the corrosion resistance and mechanical properties of the AA7075, reporting that the best combination of these properties is achieved with pre-aging at 120 ºC for 16 h, retrogressing at 200 ºC for 8 min, and re-aging at 120 ºC for 24 h.

Although the heat treatments mentioned above are those commonly used in the industry, recently a number of papers have been published highlighting the benefits of other treatments, or combinations of them, on the mechanical properties of AA7075 alloy. The effect of W-temper heat treatment (solution and rapid cooling) and the simulation of such temper on the mechanical properties and fracture was presented by Moon et al [16] reporting formability improvements over T6, and a localized ductile fracture condition immediately after treatment, different from the brittle fracture condition shown by T6. A study on fracture surface properties of 7075-T651 aluminium alloy under different load conditions and under strain-controlled conditions was presented by Macek et al [17], concluding that the values of the fracture surface parameter, core height, found in the two-stage loading program depend linearly on the equivalent strain, and logarithmically on the fatigue life. Other work on fatigue crack propagation in these alloys is presented in reference [18]. Kumar et al [19], by mechanical and metallographic testing, investigated the effect of Deep Cryogenic Treatment (DCT) on the mechanical and ballistic properties of AA7075-T6 alloy, finding an increase in tensile strength, impact strength and microhardness of AA7075-DCT samples compared to the base material (AA7075-T6) samples; while metallographic analysis revealed fine grains and secondary phase particle distribution in the microstructure of AA7075-DCT samples. They concluded that DCT improved the mechanical and ballistic properties of the aluminum alloy due to grain refinement and high dislocation density.

In this work, using an AA7075 alloy of the same origin and considering the synthesis process, the provenance of the alloy, the heat treatments applied, and the microstructure of the sample, we carried out a comparative study of the mechanical properties and the fractography of this alloy when subjected to T6, T7, and RRA treatments.

2. MATERIALS AND METHODS

2.1 Commercial alloy AA7075

A commercial aluminum alloy AA7075, supplied by SUMINDU, S. A., Barcelona, Anzoátegui, Venezuela (bars Ø = 25.4 mm), was used in this study. Its chemical composition in percentage by weight (% by weight) is shown in Table 1.

2.2 Methodology

The specimens were tension tested and machined to standardized dimensions as per ASTM E8/E8M09 (ASTM E8, 2009), as shown in Figure 1.

Table 1. Nominal composition, in % by weight of commercial alloy AA7075.

	Al	*Zn*	*Mg*	*Cu*	*Fe*	*Si*	*Mn*	*Cr*	*Ti*
Máx	Remainder	6.1	2.9	2.0	0.5	0.4	0.3	0.28	0.2
Min		5.1	2.1	1.2				0.18	

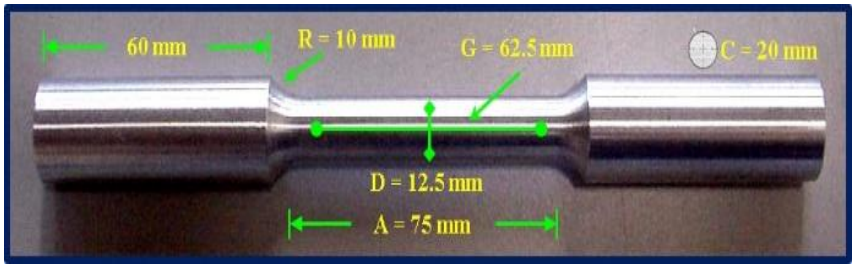

Figure 1. AA7075 specimen cut and machined to ASTM E8/E8M09 dimensions. G: length between points or calibrated length, A: length of the reduced section, D: diameter of the reduced section, R: radius of curvature, C: diameter of the final section.

Once the specimens were obtained, they were homogenized at 480 ºC for 30 min and quenching in cold water (3 ºC) to minimize their microstructural evolution. The homogenized samples were subsequently subjected to the different heat treatments:

T6: aged at 25 ºC for 2 h → aged at 100 ºC for 6 h → aged at 140 ºC for 15 h.

T7: aged at 25 ºC for 2 hours→ aged at 170 ºC for 6 hours.

RRA: aged at 120 ºC for 24 h→ retrogressed at 200ºC for 40 min →re-aged at 120 ºC for 24 h.

Three specimens were used at each step for each heat treatment applied, then tested in a Zwick/Roell model Z1200E tension tester. The results of the tensile test and applied load vs. specimen elongation were digitally recorded. Stress-strain data were recorded using an MacroXten II extensometer with a maximal measurement range of 150 mm attached directly to the specimen, being his accuracy class 0.5 ISO 9513, with a maximum error ±1 µm in the differential displacement measurement between two measurement points in the range of 20 µm to 200 µm. Tests were stopped when total fracture occurred in each specimen.

In each case, fractographies of the heat-treated specimens, once fractured, were observed in a PHILLIPS scanning electron microscope model FEI QUANTA 200 with an accelerating voltage of 20 kV (Figure 2).

Figure 2. AA7075-T6 fractured specimens obtained at the end of the tensile test.

3. RESULTS AND DISCUSSION

3.1 Tensile test

True stress versus true strain (σ vs ε) graphs showing the elastic and plastic zones characteristic of the materials were obtained from the tensile test. Figures 3, 4, and 5 show the σ vs ε graphs for AA7075 subjected to homogenization, T6, T7 and RRA heat treatments, respectively. They show the curves corresponding to three specimens for each of the thermal conditions to which the alloy was exposed. The average values of the mechanical properties were obtained from these graphs: yield stress ($\sigma_{y0,2\%}$), tensile strength (S_{UTS}), true stress at maximum load (σ_u), fracture stress (σ_f), ductility (% L and % A), resilience modulus (U_R), and toughness (U_T). Table 2 summarizes the values of the mechanical properties of AA7075 subjected to different heat treatments, in each case the measurements are affected by an error of less than 2%, estimated according to reference [20].

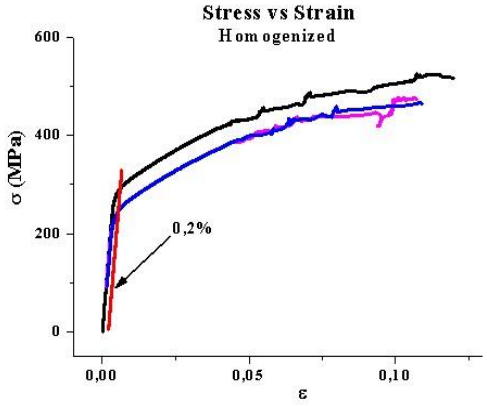

Figure 3. True stress-strain curves corresponding to a homogenized commercial alloy AA7075. Specimens — *1*, — *2*, — *3*.

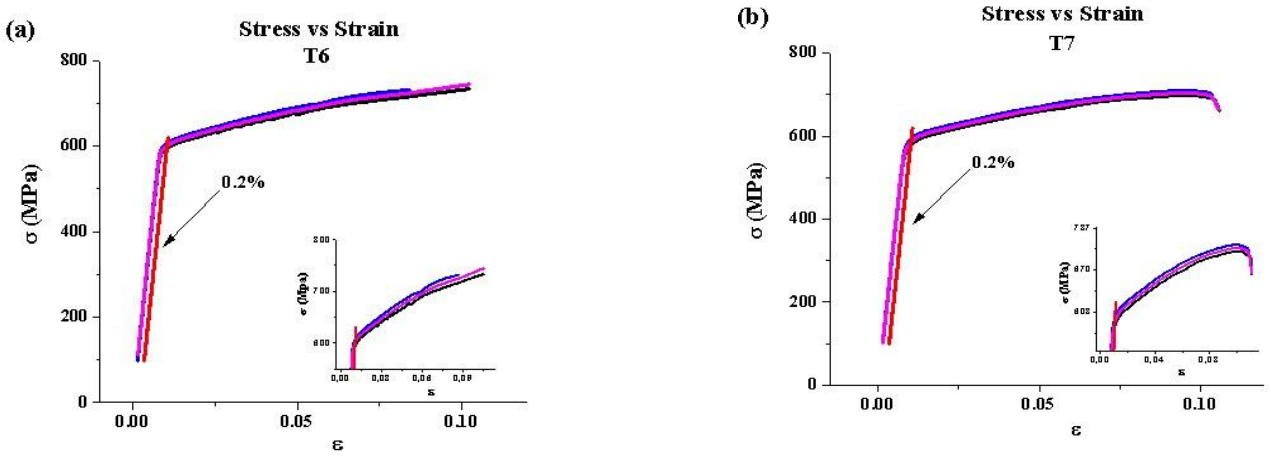

Figure 4. True stress-strain curves corresponding to AA7075 subjected to heat treatments: (a) T6 (b) T7. Specimens: — *1*, — *2*, — *3*. Insert: Enlargement of the plastic zone of the alloy.

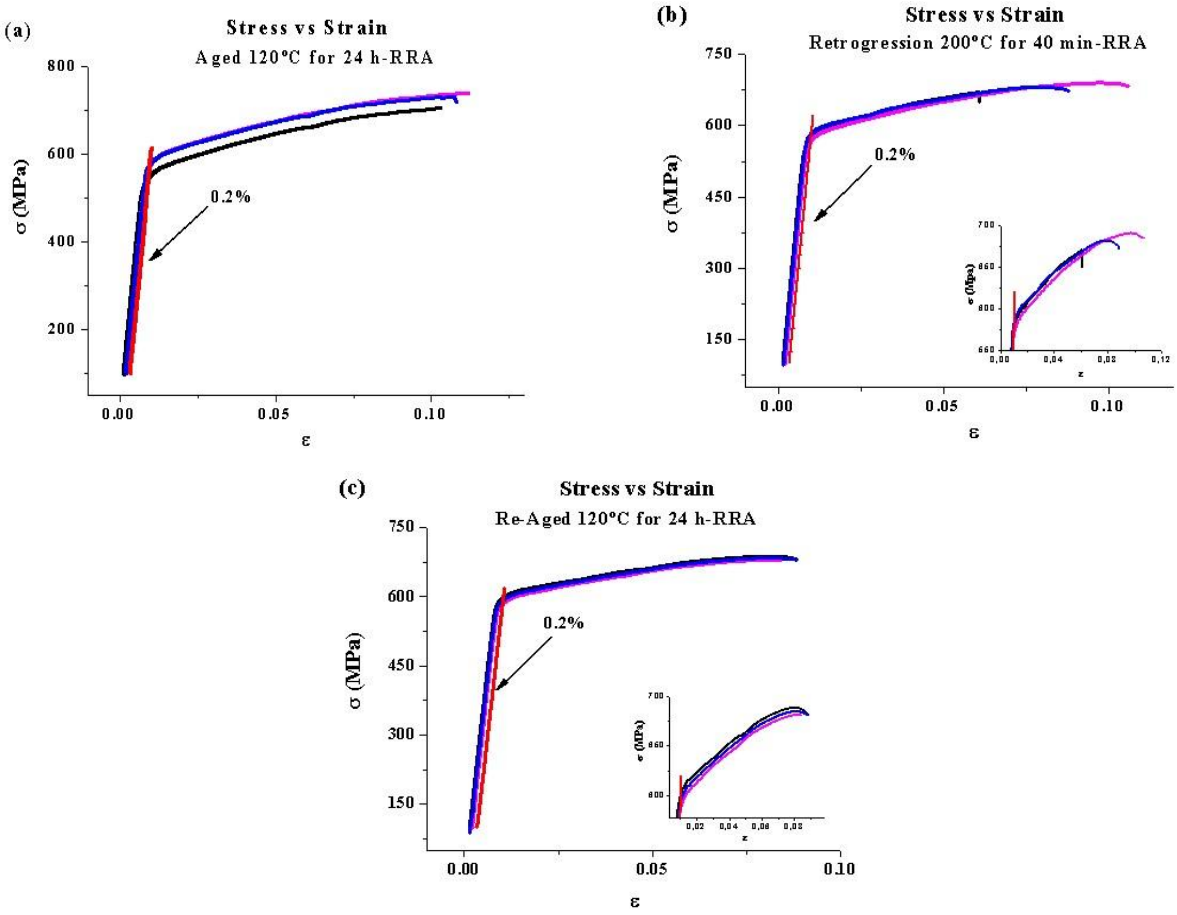

Figure 5. True stress-strain curves corresponding to commercial alloy AA7075 in each of the stages of the RRA treatment: (a) Aged, (b) Retrogression (c) Re-Aged. Specimens: — *1*, — *2*, — *3*. Insert: Enlargement of the plastic zone of the alloy.

An increase in the values of static properties $\sigma_{y0,2\%}$, S_{UTS}, σ_u, σ_f of the heat-treated AA7075 alloy relative to the values obtained from the as-delivered condition specimen (specimen without TT) is reported. The percentage increase for yield stress ranged between 8 % (T7) and 11 % (T6); for S_{UTS}, between 6 % (RRA) and 12 % (T6); for true stress at maximum load, between 7 % (RRA) and 15 % (T6); and for σ_f, between 9 % (T7) and 20 % (T6). The U_R modulus grew between 12 % (Retrogression) and 22 % (T6) with respect to the specimen without TT. This means that AA7075 is one of the Al alloys that undergo an increase in their mechanical strength when subjected to heat treatments; especially T6, since a fine precipitation of η' particles in the matrix is obtained with this treatment, which helps improve its microstructural condition. However, the values of ductility and toughness of the AA7075 alloy decreased from 33% and 39 % (Retrogression step in RRA treatment) to 6 % (T7) and 26 % (Retrogression), respectively. The increase of the mechanical strength in the alloy produced a decrease in its ductility and toughness, a behavior also reported in other materials [21].

The homogenized samples showed a decrease in their mechanical properties, ductility being reduced by up to 3 % and U_R by up to 77 %. The reason for this drastic change in the mechanical properties of the homogenized AA7075 with respect to the delivery sample is associated with the difference in microstructure in both samples. As we established in our previous work [1,2], the homogeneous microstructure of our alloy shows only incipient traces of Guinier-Preston zones formed during quenching, whereas the delivery sample and the heat-treated samples have a series of precipitates typical of each treatment; and distributed in type, shape, and size accordingly [1,2].

Table 2. Mechanical properties of commercial alloy AA7075 subjected to different heat treatments.

Heat Treatment		$\sigma_{y0,2\%}$ *(MPa)*	S_{UTS} *(MPa)*	σ_u *(MPa)*	σ_f *(MPa)*	*Ductility*		U_R *(MPa)*	U_T *(MPa)*
						%L (%)	*%A (%)*		
Specimen without HT		544	596	636	557	6	8	2	73
Homogenized		260	443	488	434	5	8	0.47	42
T6		601	667	732	667	4	8	2	62
T7		586	644	697	606	4	8	2	68
RRA	Aged 120ºC for 24 h	568	654	716	647	4	8	2	69
	Retrogression 200ºC for 40 min	574	631	677	614	3	8	2	54
	Re-Aged 120ºC for 24 h	591	634	680	625	4	8	2	55

In general, since all the reported variations of the mechanical properties are a consequence of the interaction between the different elements making up the microstructure [9], they constitute a logical and coherent explanation of precipitate redistribution.

The η'/η ratio in T6 and T7 treatments can induce higher mechanical strength thanks to the presence of aging peaks (T6) or an over-aging that yields maximum rupture strength and higher corrosion resistance (T7) thanks to the higher abundance of η' precipitates and their smaller size in T7 as compared to T6. RRA induces improvements in both properties as it regulates the type and proportion of precipitates

and defects within the grain and its vicinity [1,2,22].

Young's modulus was evaluated in the elastic zone, showing minimal variations, which are within the statistical range of the value established in the literature. These values are shown in Table 3.

Figures 6 and 7 show the plastic region of the real stress-strain curve of alloy AA7075 subjected to different heat treatments and the three curves plotting the average of the three specimens for each thermal exposure. The plastic properties of the alloy, given in Table 3, were obtained from these graphs. The values obtained from Hollomon's law for strain work-hardening exponent n and plastic modulus K for thermal treatments T6, T7, and RRA, as compared to those undergone by the delivery specimen, underwent increases, AA7075-H prevailing with the highest n value (n = 0.23) and AA7075T6 dittoing with K (K = 922 MPa). The higher hardening coefficient of AA7075-H might be the result of the precipitation of the Cu-rich S-phase (Al_2CuMg) at approximately 480 °C [23], an ideal temperature for the homogenization of AA7075. The value of K in the AA7075T6 alloy confirmed once again that T6 is the heat treatment that substantially improves the mechanical strength of the alloy.

Figure 8 summarizes the mechanical properties of the alloys. The stress and mechanical properties (yield stress and tensile strength) of the alloy subjected to TT-T6 reveal higher values than those obtained with the other heat treatments. In contrast, the properties of the homogenized alloy reported the lowest values. The differences observed are predicated on the microstructural conformation each treatment generates in the alloy.

Figure 8 highlights the higher tensile strength obtained with T6 and the higher toughness obtained with T7.

Table 3. Tensile elasto-plastic parameters of commercial alloy AA7075 subjected to different heat treatments.

Heat Treatment		Hooke's Law (elastic zone $\sigma = E\,\varepsilon$)			Hollomon's Law (plastic zone $\sigma = K\,\varepsilon^n$)		
		E (GPa)	b	R^2	n	K (MPa)	R^2
Specimen without HT		73.3	–5.81089	0.9996	0.08	798.8	0.991
Homogenized		72.3	2.91976	0.9996	0.23	809.3	0.994
T6		73.1	3.39386	0.9999	0.10	921.9	0.989
T7		71.0	4.71875	0.9998	0.08	859.8	0.991
RRA	**Aged 120ºC for 24 h**	73.1	–52.54114	0.9999	0.11	920.4	0.993
	Retrogression 200ºC for 40 min	72.6	–50.75849	0.9999	0.09	848.1	0.994
	Re-Aged 120ºC for 24 h	72.8	4.21983	0.9999	0.07	822.4	0.990

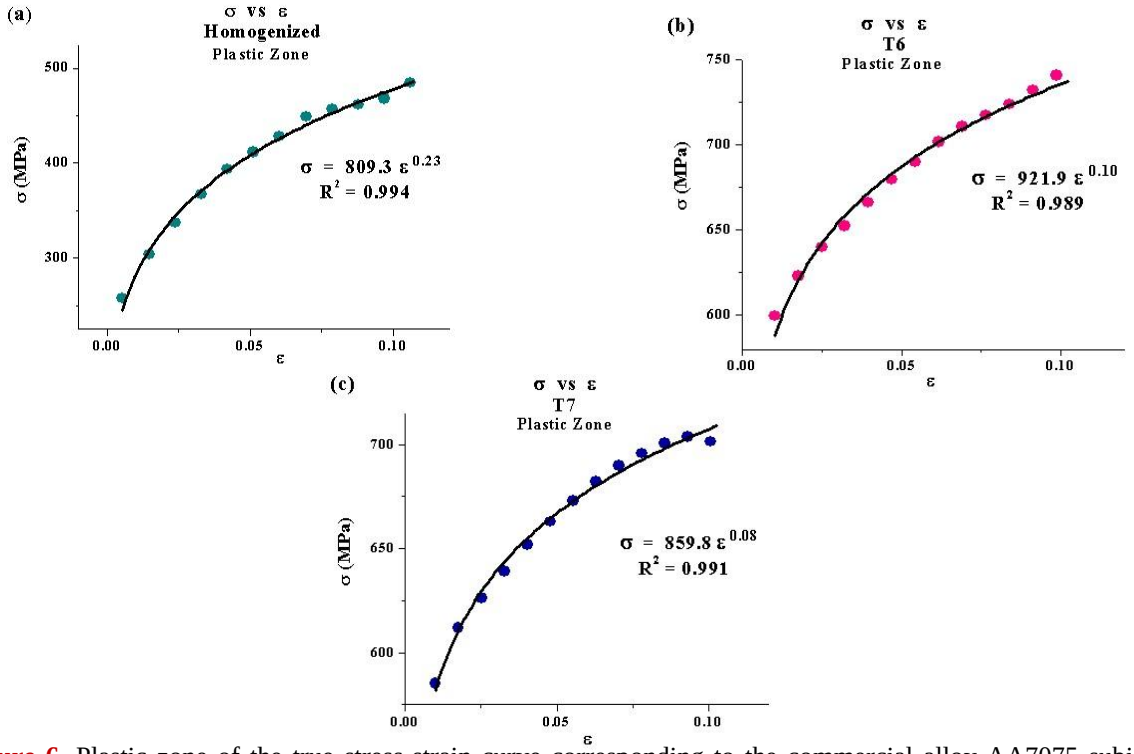

Figure 6. Plastic zone of the true stress-strain curve corresponding to the commercial alloy AA7075 subjected to heat treatments: (a) Homogenization, (b) T6 and (c) T7. ● Experimental, —— Polynomial (Hollomon).

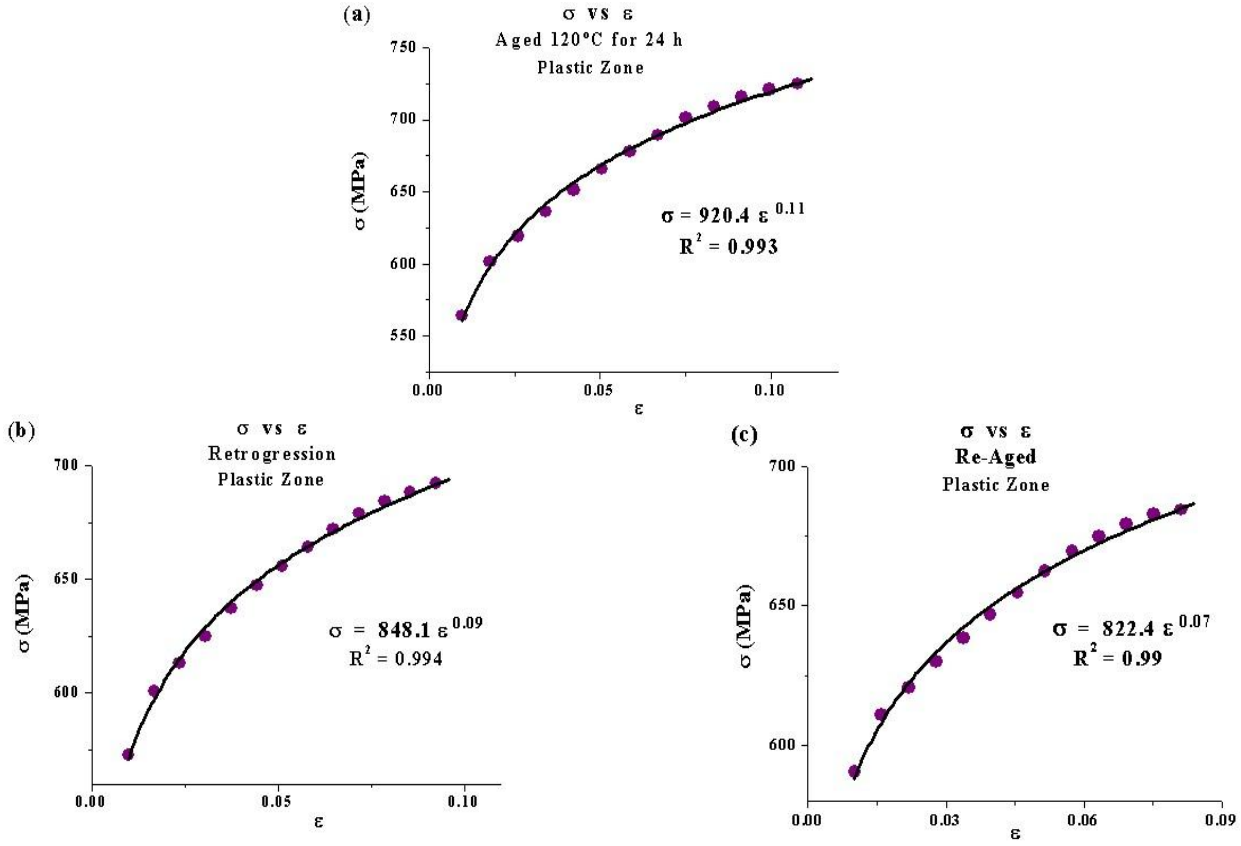

Figure 7. Plastic zone of the real stress-strain curve corresponding to the commercial alloy AA7075-RRA: (a) Aged (b) Retrogression, and (c) Re-Aging. ● Experimental, ——Polynomial (Hollomon).

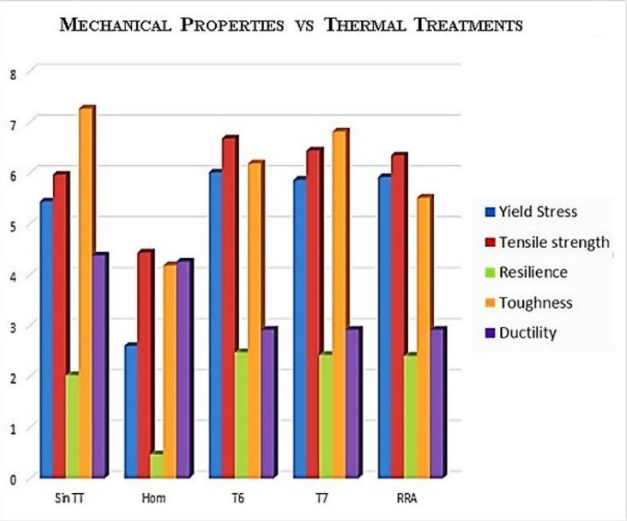

Figure 8. Comparative graph of the mechanical properties of commercial alloy AA7075 as a function of the heat treatments applied.

3.2 Fractographic study of alloy AA7075

For the fractographic analysis corresponding to the tensile test, one specimen was chosen for each step of every heat treatment applied.

3.2.1. Tensile test of a AA7075 specimen without heat treatment

Figure 9.a shows the fractography of the facture surface cross-section, which broadly reflects the ductile character of the failure showing the decreased area resulting from the perpendicular stress applied to it. Figures 9.b and 9.c show SEM micrographs of an enlarged area of the specimen tested. These figures show transgranular cracks and some micro-concavities possibly formed by localized dimple colonies, which become secondary cracks because of the stress applied.

The fracture surfaces present an irregular distribution in shape, size, and dimple scarcity, most of them lacking precipitates in their interior, a fact reflected in the high toughness shown in Table 2 and Figure 8. Some zones on the fracture surface are shown smooth, without dimples, a consequence of friction during the fracture process [24]. Although the behavior reflected in this micrograph is typical of ductile materials [25-28], the mechanism responsible for the fracture of the samples seems complex, involving dimple coalescence and matrix stretching brought about by the friction and stress generated by the dimples and microcavities in their environment. This behavior is very similar to that reported in Reference [11] in deformed samples and attributed to quasi-cleavage.

3.2.2. Tensile test of a specimen of the AA7075-homogenized alloy

Figures 10 (a-c) correspond to SEM fractographies of the facture surface cross-section of the homogenized AA7075 and their respective magnification. The magnification evinces the presence of transgranular cracks and a wide dimple distribution throughout the fractured surface, which confirms the ductile nature of such fractures [28]; dimple nucleation, growth, and subsequent coalescence being the dominant fracturing mechanism in the specimens. Irregularly shaped particles are also observed both at the contours and inside the dimples (Figure 10.c). The EDX spectra of two of these particles are shown in Figure 10.d, the lines of greater intensity corresponding to Al and Mg. The elements Cu, Zn, Mg, Fe, and Mn, among others, are also identified. It is worth noting that the presence of Cu rich phases (S-Al_2CuMg phase) has been identified in samples treated at high temperatures [1,29].

3.2.3. Tensile test of AA7075-T6 alloy specimen

Figures 11 (a-c) are SEM micrographs of the AA7075-T6 alloy subjected to a tensile test. These micrographs correspond to the cross-section and expanded area of the specimen tested. As the magnification is increased, intergranular cracks with irregularly shaped and sized micro dimples, characteristic of ductile fractures, can be observed [25]. Some secondary cracks are also identified in these micrographs. An important presence of precipitates, distributed throughout the fracture surface and located both inside and outside the dimples, is also identified. The EDX spectra of two of these particles, shown in Figure 11.d, exhibit a majority presence of Al and Mg and, in a smaller proportion, the presence of Zn, Cu, Si, Fe, Cr; and particularly, oxygen and carbon, the latter entered during the manipulation of the specimens. The fracture mechanism seems to be like that of the homogenized samples, although the precipitates and dimples present a smaller size due to aging at 140°C.

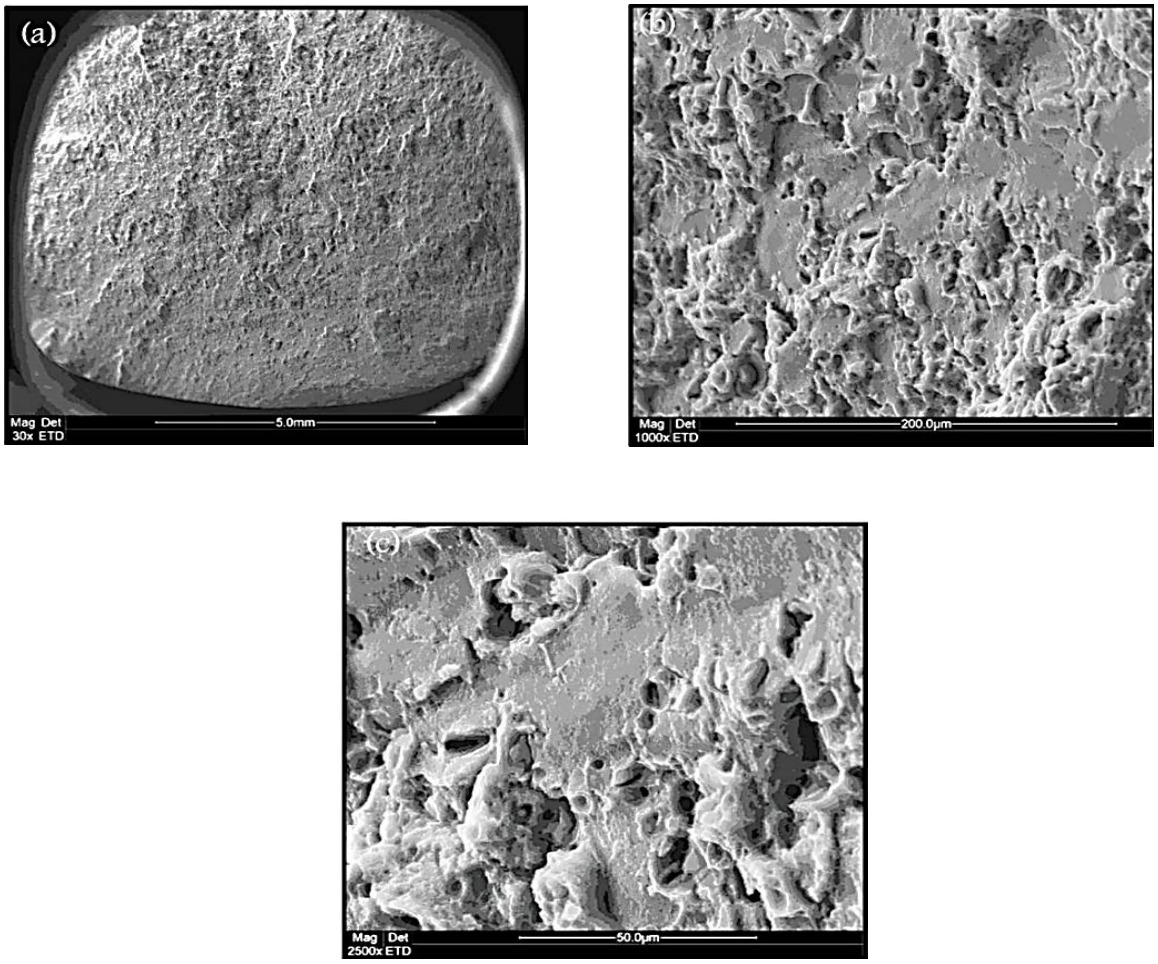

Figure 9. SEM micrographs of a commercial AA7075 alloy without TT subjected to a tensile test: a) fracture surface cross-section of the specimen b) midsection of the fractured surface, and c) enlargement of the fractured surface's midsection.

3.2.4. Tensile tested specimen of the AA7075-T7 alloy

Figures 12 (a-c) are SEM fractographies of the AA7075-T7 tested by following the same protocol of the previously studied samples. The enlargement shows evidence of transgranular cracks [25] and dimples distributed over the entire fracture surface and having a larger diameter than those reported for the AA7075-T6 alloy. The contrast in the figure hints at the presence of microcavities. The fracture is of a ductile character, and some particles are observed inside the dimples (Figure 12.c). Precipitates rich in Al, Cu, Zn, Mg, Mn, and Fe are predicted from the EDX spectra highlighted in Figure 13.d. Note that the specific spectra in this figure differ from those shown for the T6 treatment because the temperature and aging time in both treatments facilitate the formation of different precipitates, T7 favoring abundant precipitation of the η' phase.

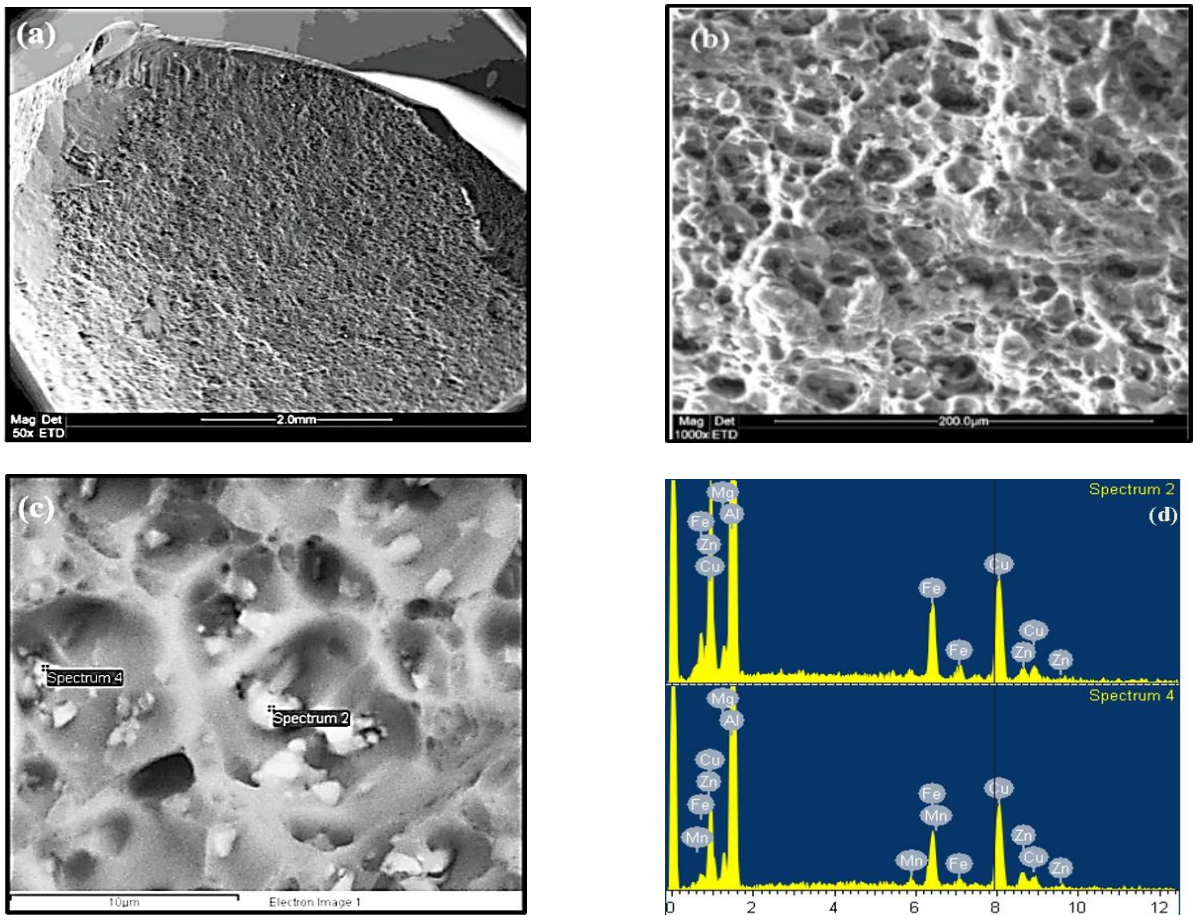

Figure 10. SEM micrographs of a homogenized commercial AA7075 alloy subjected to a tensile test: a) Cross-section of its fracture surface, b) segment of the central zone of the fracture surface, and c) enlargement of the central zone of the fracture surface. d) EDX spectra in two particles of the alloy studied.

3.2.5 Tensile test of alloy AA7075 specimen subjected to RRA heat treatment

Fractographies corresponding to the steps composing the RRA heat treatment are shown in Figure 13.

These micrographs show overall ductile transgranular failures modeled at each step by the heat treatment applied.

Figures 13 (a-c) correspond to SEM micrographs of the AA7075 alloy aged at 120 ºC for 24 h. A tangle of dimples very similar to that observed in the specimens subjected to T6 is evidenced, their enlargement showing an irregular distribution and important size and depth. This behavior is no doubt related to the high ductility and toughness reflected in Table 2. The local composition of two of them, analyzed by EDX, whose spectra are shown in Figure 14, indicates the important participation of Al and Mg, in addition to Fe, Zn, Cu, and Mn, among others.

Figures 13 (d-f) correspond to samples subjected to retrogression at 200 °C for 40 min. The micrographs are somewhat related to what was observed in the specimens subjected to T7, with a higher dimple density of smaller size and precipitates located throughout the fracture surface. Some microcavities, indicative of possible cleavage [24], are also exposed. Micrograph 13.d details the presence of precipitates of semi-spherical morphology located preferentially on the outside of the dimples.

.

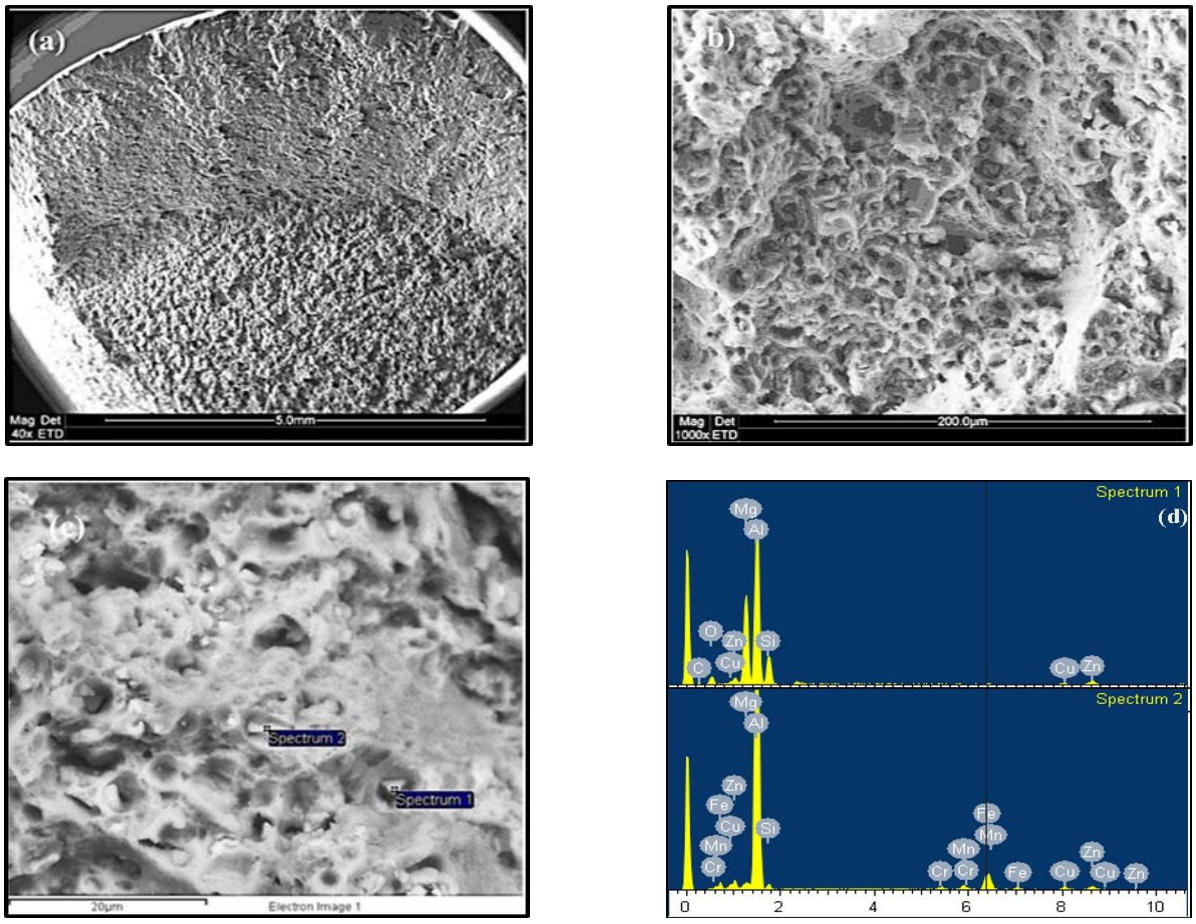

Figure 11. SEM micrographs of a commercial AA7075 alloy aged at 140 ºC for 15 h (T6) and subjected to a tensile test: a) Cross-section of the fracture surface of the specimen, b) segment of the central zone of the fractured surface, and c) enlargement of the central zone of the fracture surface. d) EDX spectra in two particles of the alloy studied.

Figures 13 (g-i) correspond to the cross-section and enlarged area of the re-aged AA7075 fracture surface, the last step of the RRA treatment. As magnification increases, the transgranular character of the cracks becomes visible, and so do microholes of varying sizes, typical of ductile materials. As for the particles located within these microholes and on their contours, the EDX spectra of Figure 14.i show that they are precipitates rich in Al, Mn, Fe, Mg, Zn, and Cu.

Our fractographic study reveals that the thermal treatments affect the distribution, number, and size of dimples; and when related to the values of the mechanical strength of the AA7075 tested, given in Table 2, it is confirmed that the greater the number of micro dimples, the lower the ductility of the sample and the higher its mechanical strength.

4. CONCLUSIONES

The commercial alloy AA7075 was subjected to RRA, T6, and T7 heat treatments and assessed by tensile testing and SEM techniques to evaluate their effect on its mechanical properties, behavior, and fractography. The results show that:

1. The thermal treatments condition the microstructure of the alloy, generating different phases whose shape and size distribution regulate its mechanical properties.
2. The homogenized samples were the most ductile (together with the samples originally delivered) as well as the least resilient and tenacious.

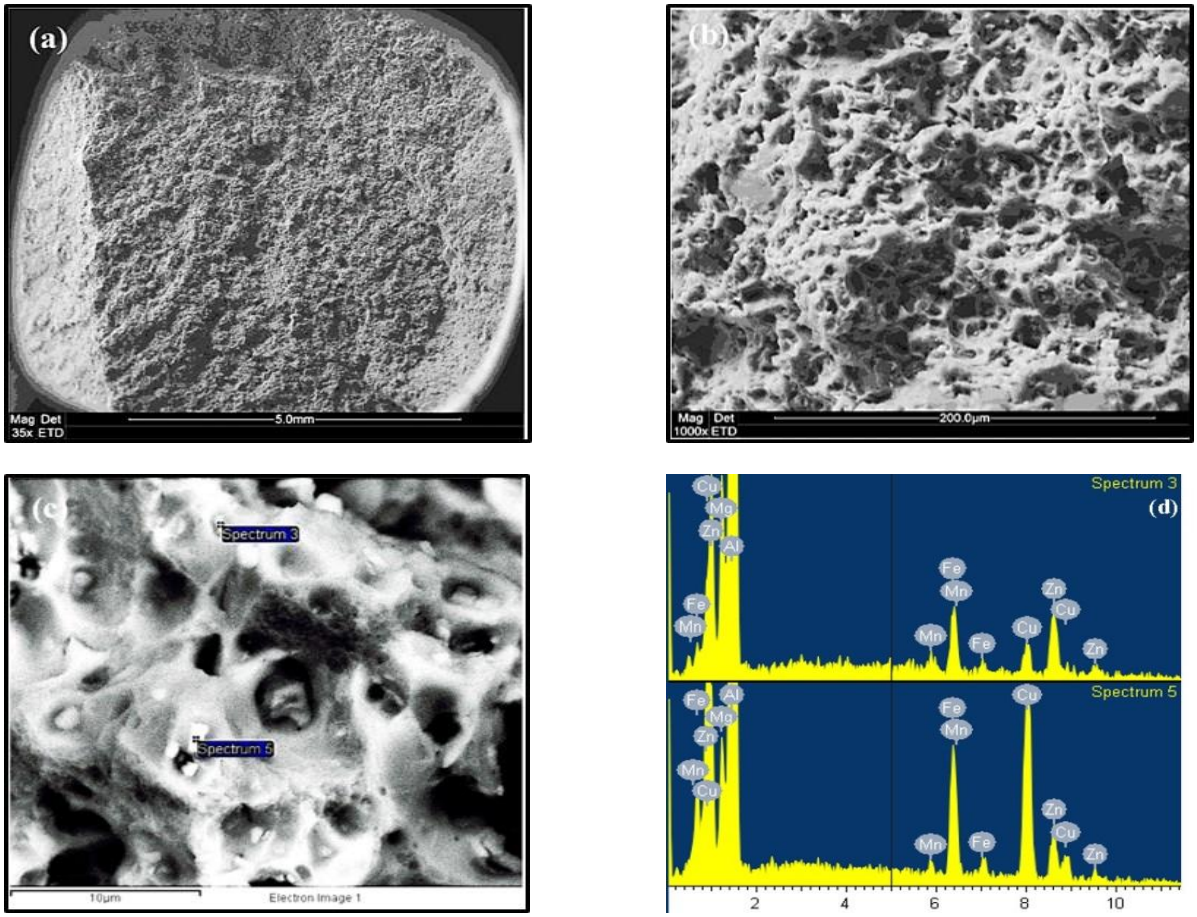

Figure 12. SEM micrographs of a commercial AA7075 alloy aged at 170 ºC for 6 h (T7) subjected to a tensile test: a) Cross-section of the fracture surface of the specimen, b) segment of the central zone of the fracture surface, and c) enlargement of the central zone of the fracture surface. d) EDX spectra in two particles of the alloy studied.

3. The T6 treatment enhances all the mechanical properties of the alloy except its toughness, which is lower than that shown by samples subjected to T7.
4. The RRA treatment induces a behavior of the mechanical properties intermediate between T6 and T7, which makes it possible to regulate the corrosion resistance in T6 and the overexposure of T7.
5. The fractographic study reveals the ductile and transgranular character of the fractures studied, the formation, growth, and coalescence of microholes being responsible for such fractures in the heat-treated samples. In the untreated samples, a complex behavior associated to the high presence of defects was detected, a phenomenon that hints at the possible existence of quasi-cleavage.
6. The thermal treatments modify the distribution, size, and shape of dimples, affording ductility to the fracture.
7. As the number of micro dimples in the alloy, increases because of the tempers applied, its ductility decreases, and its mechanical resistance improves. Some researchers associate this characteristic with the presence of precipitates inside the microholes; our micrographs, however, reveal the presence of precipitates, mainly rich in Al and Mg and distributed over the entire fracture surface.

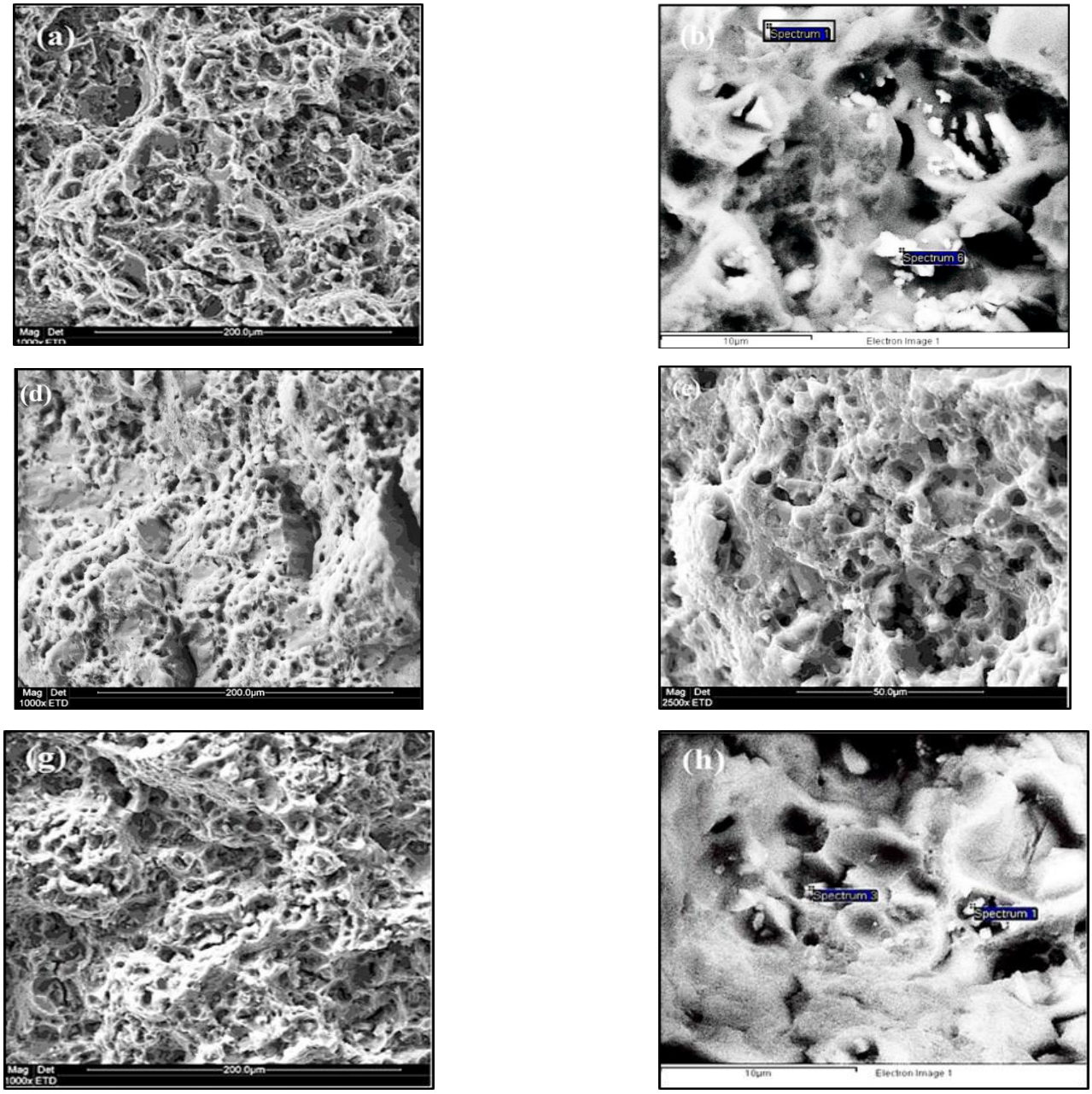

Figure 13. SEM micrographs of a commercial AA7075-RRA alloy showing the effect of the tensile test at each step of the heat treatment. First line (a, b): 1st RRA step (aging at 120ºC for 24 h). Second line (d, e): 2nd RRA step (retrogression at 200ºC for 40 min). Third line (g, h): 3rd RRA step (re-aging at 120ºC for 24 h).
a, d, g: Segment of the central zone of the fracture surface. b, e, h: enlargement of the central zone of the fractured surface. (c, i) in Figure 14 : EDX spectra in two particles present in the alloy studied, correspondent to RRA first step and RRA final step,

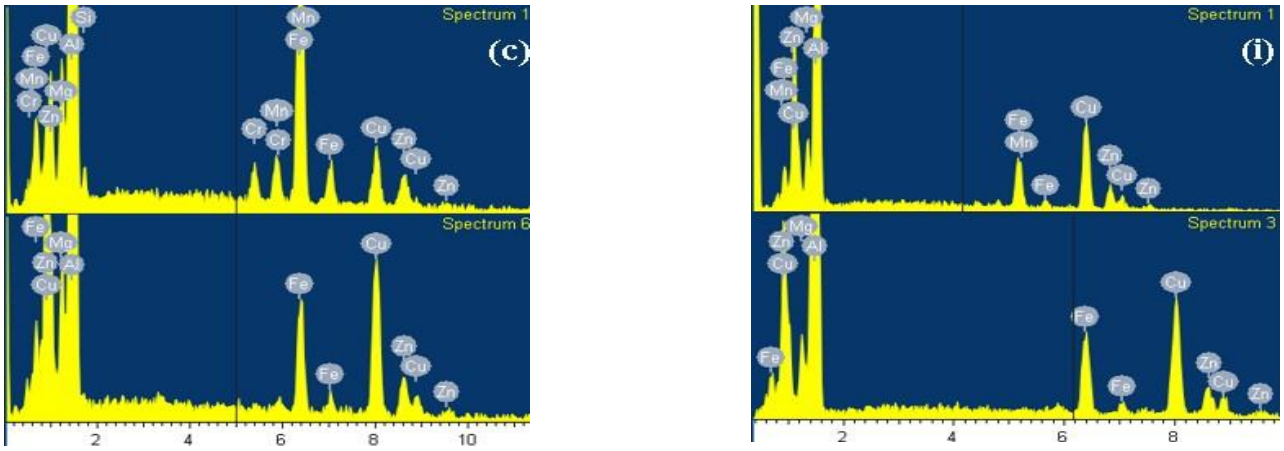

Figure 14. SEM-EDX spectra in two particles present in the alloy studied, correspondent to RRA first step (c) and RRA final step (i).

5. ACKNOWLEDGMENTS

The authors thank Carlos Mota for his support and translation of the manuscript. To the Research Institute of Biomedicine and Applied Sciences "Dra. Susan Tai" (IIBCA-UDO) for allowing me to use the universal mechanical testing equipment to carry out the tensile tests. To the Siderúrgica del Orinoco (SIDOR) for carrying out the SEM fractographies.

6. BIBLIOGRAPHY

[1] Luiggi NJ, Valera MV. J. Therm. Anal. Calorim. 2017; 130 (3): 1885–1902.

[2] Luiggi NJ, Valera MV. Rev. LatinAm. Metal. Mat. 2017; 37 (2): 160–178.

[3] Bhandarkar MD, Lisagor WB. NASA Technical Paper 1086. 1977.

https://ntrs.nasa.gov/api/citations/19840003162/downloads/19840003162.pdf

[4] Lynch SP, Moutsos S. J Fail. Anal. and Preven. 2006; 6 (6): 54–69.

[5] Pantazopoulos GA. Metals. 2019; 9 (148): 1–20.

[6] Hunter MS, McMillan JC, "Fractography and Microstructure of Aluminum Alloys 7075-T651 and 7075-T7351". In: The Symposium on Electron Fractography was presented during the Seventieth Annual Meeting of the Society held in Boston, Mass., 25—30 June 1967. Electron Fractography, ASTM Spec. Tech. Publ., 1968; 436: 196–211.

[7] Kirman I. Metall. Trans. 1971; 2: 1761–1770.

[8] Irisarri AM and Atxaga G, "Fractographic study of two damage tolerant aluminium alloys". In ECF13 (13th European Conference on Fracture "Fracture Mechanics: Applications and Challenges"), San Sebastian (España) 2000. Last modified: 2013-02-09: p. 1–8.

https://www.gruppofrattura.it/ocs/index.php/esis/ECF13/paper/viewFile/8505/4947

[9] Zhihui L, Xiong B, Zhang Y, Zhu B, Wang F, Liu H. Mater. Charact. 2008; 59: 278–282.

[10] Panigrahi SK, Jayaganthan R. Mater. Sci. Forum. 2008; 584-586: 734–740.

[11] Tajally M, Huda Z, Masjuki HH. J. Appl. Sci. 2009; 9 (21): 3888–3893.

[12] Pedersen KO, Børvik T, Hopperstad OS. Mater. Des. 2011; 32 (1): 97–107.

[13] Askari-Paykani M, Meratian M, Shayan M, Raeissi K. Anti-Corros. Methods Mater. 2012; 59 (5): 231–238.

[14] Carvalho ALM, Martins JP, Salvati E, Sui T, Korsunsky AM. Procedia Struct.Integr. 2016; 2: 3697–3704.

[15] Li R, Liu T, Su R, Su J, Qu Y. J. Mater. Eng. Perform. 2018; 27 (11): 6246–6255.

[16] Moon C, Thuillier S, Lee J, Lee MG. J. All. Com. 2021; 856: 158180

[17] Macek W., Branco R, Costa JD, Pereira C. Mech. Mat. 2021; 160: 103972

[18] Branco R, Costa J.D, Borrego L.P, Wu S.C, Long X.Y, Zhang F.C. Int. J. Fatig. 2019; 129: 105234.

[19] Kumar SD, Magarajan U, Kumar SS, Rodríguez M. D. T. 2023; 30: 101-110

[20] Kostic S, Miljojkovic J, Simunovic G, Vukelic J, Tadic B. Eng. Sci. and Techn. An International Journal. 2022; 25, 10098.

[21] Forn A, Martín E. "Resistencia y flujo plástico del material compuesto 2124/SiC/17p". 2004. www.gef.es/congresos/20/pdf/GEF083.pdf

[22] Valera M del V, Luiggi NJ. Acta Microsc. 2016; 25 (1): 1–8.

[23] Belov NA, Eskin DG, Aksenov AA. Multicomponent phase diagrams: applications for commercial aluminum alloys. 2005. United Kingdom: Elsevier Ltd.

[24] Dumont D, Deschamps A, Bréchet Y. Acta Mater. 2004; 52 (9): 2529–2540.

[25] Ou BL, Yang JG, Wei MY. Metall. Mater. Trans. A Phys. Metall. Mater. Sci. 2007; 38A: 1760–1773.

[26] Wang D, Ni DR, Ma ZY. Mater. Sci. Eng. A. 2008; 494A: 360–366.

[27] Wang D, Ma ZY. J. Alloys Compd. 2009; 469: 445–450.

[28] Vratnica M, Pluvinage G, Jodin P, Cvijovic´ Z, Rakin M, Burzic´ Z. Mater. Des. 2010; 31: 1790–1798.

[29] Wang K, Su R, Ma S, Qu Y, Li R. J. Mater. Eng. Perform. 2020; 29(5): 3297-3304.

7. MINI-BIOGRAPHY OF AUTHORS

María del Valle Valera Maneiro: Full Professor of the Physics Department of the Universidad de Oriente-Sucre (UDO). She graduated with a degree in Physics (UDO) with a thesis in seismology, a Master's degree in Physics (UDO) in the area of condensed matter and a Doctorate in Engineering Sciences (UCV). She is a researcher in the Physics of Metals Group, her field of study is the synthesis and characterization of Al alloys. (ORCID: 0000-0002-8300-0094)

Ney José Luiggi Agreda: Full Professor of the Physics Department of the Universidad de Oriente-Sucre-Venezuela. Degree in Physics with thesis in physical spectroscopy, DEA (Diplome d'Etudes Approfondies) in Metallurgy and Docteur de troisieme Cycle en Metallurgie Physique, both degrees from the Institute National Polytechnique de Grenoble (INPG) and the Ecole National Superieur d' Electrochimie et Electro-Metallurgie (ENSEEG), France. With updating internships at INSA Lyon-France. He is currently the Coordinator of the Metals Physics Group of the Physics Department of the Science School and Coordinator of the Metals Research area in the Materials Science Doctorate at IIBCA-UDO. His research field covers different topics of Condensed Matter Physics, with special interest in: experimental and theoretical characterization of Aluminum, Iron and Magnesium alloys, ab-initio calculations of electronic charge density dependent properties and Simulation of phase change kinetics by cellular automata and stochastic methods. (ORCID: 0000-0002-0215-1318)